Optimal Scheduling of Bevacizumab and Pemetrexed/cisplatin Dosing in Non-Small Cell Lung Cancer

Benjamin K Schneider, Arnaud Boyer, Joseph Ciccolini, Fabrice Barlesi,
Kenneth Wang, Sébastien Benzekry, Jonathan Paul M. Mochel

Optimal Scheduling of Bevacizumab and Pemetrexed/cisplatin Dosing in Non-Small Cell Lung Cancer

Benjamin K Schneider[1], Arnaud Boyer[2,3], Joseph Ciccolini[2], Fabrice Barlesi[3], Kenneth Wang[4], Sebastien Benzekry[1,5]* and Jonathan P Mochel[1]*

(1) Iowa State University College of Veterinary Medicine, Ames, IA, U.S.A, (2) SMARTc Unit, Centre de Recherche en Cancérologie de Marseille UMR Inserm U1068, Aix Marseille University, Marseille, France (3) Multidisciplinary Oncology and Therapeutic Innovations Department, Assistance Publique Hôpitaux de Marseille, Marseille, France, (4) Mayo Clinic, Rochester, MS, U.S.A, (5) Team MONC, Inria Bordeaux Sud-Ouest, Institut de Mathématiques de Bordeaux, France. *: co-last authors.

Correspondence:

Jonathan P. Mochel, DVM, MS, Ph.D, DECVPT

Associate Professor of Pharmacology

Iowa State University College of Vet. Medicine

2448 Lloyd, 1809 S Riverside Dr.

Ames, IA 50011-1250

Phone 515-294-7424

Email: jmochel@iastate.edu

Sebastien Benzekry, Ph.D

Associate Professor of Applied Mathematics

Team MONC, Inria Bordeaux Sud-Ouest, France

Email: sebastien.benzekry@inria.fr

Abbreviations

adm: Administer, administered, administration, etc.

BIC: Bayesian Information Criteria

BSA: Body Surface Area

CT: Combination Therapy

DNA: Deoxyribonucleic acid

Gap: Short for the administration gap between (first) bevacizumab and (second) pemetrexed/cisplatin

IP: Intraperitoneal

IIV: Inter-individual variability

IV: Intravenous

NSCLC: Non-Small Cell Lung Carcinoma

PD: Pharmacodynamic

PK/PD: Pharmacokinetic/pharmacodynamic

PEM/CIS: Pemetrexed/cisplatin

BEV-PEM/CIS: Pemetrexed/cisplatin-bevacizumab

PK: Pharmacokinetics

ROS: Reactive Oxygen Species

RFU: Relative Fluorescence Units

sGOF: Standard Goodness-Of-Fit

VPC: Visual Predictive Check

Abstract

Bevacizumab-pemetrexed/cisplatin (BEV-PEM/CIS) is a first line therapeutic for advanced non-squamous non-small cell lung cancer (NSCLC). Bevacizumab potentiates PEM/CIS cytotoxicity by inducing transient tumor vasculature normalization. BEV-PEM/CIS has a narrow therapeutic window. Therefore, it is an attractive target for administration schedule optimization. The present study leverages our previous work on BEV-PEM/CIS pharmacodynamic modeling in NSCLC-bearing mice to estimate the optimal gap in the scheduling of sequential BEV-PEM/CIS. We predicted the optimal gap in BEV-PEM/CIS dosing to be 2.0 days in mice and 1.2 days in humans. Our simulations suggest that the efficacy loss in scheduling BEV-PEM/CIS at too great of a gap is much less than the efficacy loss in scheduling BEV-PEM/CIS at too short of a gap.

Introduction

Bevacizumab-pemetrexed/cisplatin (BEV-PEM/CIS) combination therapy has been shown to be an effective first line and maintenance therapy for non-small cell lung cancer (NSCLC) in Phase II and Phase III clinical trials(1–3). Pemetrexed inhibits enzymes necessary for pyrimidine and purine synthesis – primarily thymidylate synthase, which is necessary for thymidine synthesis and tumor cell replication(4). Cisplatin is an alkylating agent which crosslinks adjacent N7 centers on purine residues, damaging DNA, disrupting repair, and disrupting purine synthesis(5–7). Disrupting DNA substrate supply results in S-phase arrest, DNA repair disruption, and eventually apoptosis(8,9). Cisplatin also significantly disrupts calcium and reactive oxygen species (ROS) regulation, inducing cellular lesions which further sensitizes cancer cells to apoptosis(7).

In contrast to the effect of PEM/CIS, i.e. DNA damage, bevacizumab is an anti-VEGF (vascular endothelial growth factor) humanized monoclonal antibody. VEGF is an angiogenic potentiator which promotes the growth of endothelial tissue necessary for arteries, veins, and lymphatics. By limiting neovascular growth, and therefore blood delivery to neoplasms, bevacizumab exhibits limited antiproliferative properties(10).

More importantly, bevacizumab transiently induces a pruning effect on neovascular beds, which normalizes blood supply to neovascularly dense tissues (i.e. tumors)(11–13). By normalizing blood supply, bevacizumab enhances chemotherapeutic (i.e. PEM/CIS) delivery to neoplasms(14,15).

The effects of BEV-PEM/CIS are generalized i.e. any cell capable of uptaking the drugs are susceptible to their effects, especially rapidly-dividing cells such as myeloid cells(16). Accordingly, BEV-PEM/CIS has a narrow therapeutic window and generalized side-effects(3). Previous studies on BEV-PEM/CIS suggest that sequential administration of BEV-PEM/CIS (i.e. BEV before PEM/CIS) outperforms concomitant scheduling of BEV-PEM/CIS in treating NSCLC(12,17–19). This makes BEV-PEM/CIS an attractive target for scheduling optimization via modeling and simulation, as a range of practical predictions – such as optimal scheduling in humans – can be made without the considerable time and resource investment required to conduct *in vivo* experiments. These predictions can be used to guide future studies, greatly accelerating drug development(20).

In our previous work on BEV-PEM/CIS published in Imbs et al. 2017(17), mice with NSCLC tumor xenografts were administered bevacizumab with PEM/CIS combination therapy (CT) in either concomitant, or delayed (i.e. bevacizumab before PEM/CIS) scheduling. The NSCLC tumors had been modified such that tumor growth could be tracked over time via either *bioluminescence* or *fluorescence*. Following previous theoretical investigations, the dataset generated from the mice with *bioluminescent* tumors was used to develop a semi-mechanistic PK/PD model for tumor dynamics in response to BEV-PEM/CIS(21,22). The model was then used to predict the optimal scheduling gap between bevacizumab and PEM/CIS administration.

The aim of this follow-up modeling work was to both refine and expand upon previous results on BEV-PEM/CIS CT using the much larger *fluorescence* dataset generated in Imbs et al. 2017(17). We first showed that the semi-mechanistic model previously developed better explained the data than comparable models (i.e. we validated the previously developed structural model). Then, we refined the parameter estimates of the model, and used it to predict the optimal scheduling gap between bevacizumab and PEM/CIS administration. Next, we used stochastic simulations to explore the marginal loss in therapeutic efficacy when BEV-PEM/CIS was administered at a sub-optimal gap, the effect of bevacizumab dose scaling on population optimal gap, as well as the inter-individual variability (IIV) of optimal gap. Lastly, using literature human PK/PD models and parameter estimates, we were able to scale the model to estimate the optimal scheduling of BEV-PEM/CIS in humans.

Methods

Experimental Procedure

Comprehensive details on animals and the experimental procedure are available in Imbs et al. 2017(17). Briefly, on Day 0 of the experiment, tumors (ca 120,000 cells) consisting of H460 human NSCLC transfected with luciferase and the tdTomato gene (H460 Luc+ tdTomato+, Perkin Elmer France) were injected ectopically into the left flank of 90 mice. Animals were pathogen-free, immunocompromised, 6-week-old, female Swiss nude mice (Charles River, France). The mice were randomized into one of five treatment groups. The first study group (Control) received no treatment. The second treatment group (PEM/CIS) was administered both 100 mg/kg of pemetrexed IP and 3 mg/kg of cisplatin IP on Days 14, 28, and 42 of the experiment. The third, fourth, and fifth treatment groups (BEV-PEM/CIS) received the same PEM/CIS treatment as the second experimental group.

In addition, the BEV-PEM/CIS treatment groups were administered 20 mg/kg IP of bevacizumab either concomitantly with the PEM/CIS administrations (Group 3), 3 days prior to each PEM/CIS administration (Group 4), or 8 days prior to each PEM/CIS administration (Group 5) – see **Table S1** for administration tabulation.

Tumor growth was monitored on a minimum bi-weekly basis using Ivis Spectrum imager (Perkin Elmer France) and images were acquired and analyzed using the Living Image 6.0. software (Perkin Elmer France).

Mice were supplied with paracetamol supplemented water (e.g. 80 mg/kg/day) to prevent disease-related pain. Animals showing signs of distress, pain, cachexia (i.e. loss of 10% of body mass), or extensive tumor proliferation (i.e. within 2-3 cm) were euthanized. All animals were euthanized on Day 87 of the experiment. All experiments were approved by the local ethical committee at French Ministère de l'Education Nationale, de l'Enseignement Supérieur et de la Recherche, and registered as #2015110616255292.

PK/PD Structural Model Building and Evaluation

The PK models for bevacizumab, pemetrexed, and cisplatin were derived from previously published PK models in mice(23–25). The parameters for these models were fixed to the typical values from those studies and assumed no IIV.

The PD model was selected from a series of sequentially fit tumor growth and drug effect models. First – using only the control dataset – the exponential, linear-exponential, and Gompertz growth model were cross-evaluated as models of unperturbed tumor growth(26). Then, incorporating the full dataset into the fit, the log-kill effect of bevacizumab, log-kill effect of pemetrexed, and log-kill effect of cisplatin were each considered. The interaction effect between bevacizumab and PEM/CIS was included to represent the synergistic effect of bevacizumab. Following previous work for the effect of cytotoxic drugs, three cellular death compartments were included in the PD portion of the model to represent the delay between cellular damage due to PEM/CIS and cell death(27).

Competing models were evaluated numerically using Bayesian information criteria (BIC) and the precision of parameter estimates – defined as the relative standard error of the estimate (RSE).

Observed vs. predicted plots, individual fit plots, and Visual Predictive Checks (VPCs) were produced to graphically assist model evaluation (as automated in Monolix 2018R2). VPCs were produced using the default estimation process for VPCs as of Monolix 2018R2 i.e. to create the 90% prediction intervals for the 10th, 50th, and 90th percentiles, 500 simulations are performed using random individual parameters and the design structure of the experiment.

After model selection, the statistical correlations between random-effects were explored via visual inspection. Correlations plots between random effects were produced, defined as η_{i,t,ϕ_1} vs η_{i,t,ϕ_2} i.e. the random effect η, of individual i, at time t, of parameter 1, i.e. ϕ_1, vs the random effect η, of individual i, at time t, of parameter 2, i.e. ϕ_2. The full posterior distribution of the parameters were used in place of EBEs to avoid visual artifacts due to shrinkage as suggested by Lavielle, et al, 2016(28) and Pelligand L, et al, 2016(29). Statistical correlations between random effects were also numerically assessed using a Pearson correlation test at a $P < .05$ threshold.

SAEM convergence and final model parameterization were graphically assessed by inspection of search stability, distribution of the individual parameters, distribution of the random effects, individual prediction vs. observation, individual fits, distributions of the weighted residuals, as well as VPCs.

The precision of parameter estimates was numerically assessed using RSE. The normality of random effects distributions, the normality of individual parameter distributions, and the normality of the distribution of residuals were each numerically assessed using a Shapiro-Wilk test ($P < .05$). The centering of the distribution of residuals (i.e. centered on 0) was numerically assessed using a Van Der Waerden test ($P < .05$).

Parameter stability was assessed by comparing parameterizations resulting from random-initial starting value selection – as implemented in the Monolix *assessment suite*. The *assessment suite* performs 5 SAEM parameterizations in series using random initial parameter values uniformly drawn from the interval from approximately 60% to 160% of final parameter estimates. The SAEM of the individual parameterizations was then tracked between runs - giving a range of parameter value estimates, RSEs, and log-likelihoods to compare. This assessment was used to ensure that the algorithm did not converge to a log-likelihood local minimum during the

process of producing final parameter estimates. The settings described are the default as of Monolix 2018R2.

Simulations

Simulations were performed in R 3.4.4 using Simulx 3.3.0(30) to simulate from Monolix run files. First, a function was built which accepted treatment schedule, parameter substitutions, dose, and number of individuals as input and produced a simulated population as an output. This function was simply a convenience wrapper of Simulx for automation purposes and was verified by reproducing VPCs per treatment group. **Simulation set 1** was used to predict the optimal gap between administration of bevacizumab and PEM/CIS. **Simulation set 2** produced an estimate of the IIV of the optimal gap. **Simulation set 3** examined the anticipated effect of varying the dose of bevacizumab on the optimal gap. **Simulation set 4** scaled predictions of BEV-PEM/CIS efficacy to humans. All simulations were of population level response (i.e. simulated without RSE or IIV) except for **simulation set 2** (simulated without RSE and with IIV) which used 1000 monte carlo samples. Further details are provided in the **supplementary methods**.

Quality assessment

All mlxtran and R codes were assessed for quality control by an independent evaluator.

Results

Error Model

Measurement error was best described using a log-normal constant-error model (**equation 1**). The natural-log of each individual measurement, $ln(y_{ij})$ with individual i and repetition j, was modeled as a measurement centered on the natural-log mean of y_{ij} over j, i.e. $ln(\bar{x}_i)$, in addition to some residual error, ϵ_{ij}, normally distributed, centered on zero, and with standard deviation a.

$$y_{ij} = \bar{x}_i \cdot e^{\epsilon_{ij}} \ \ where \ \ ln(y_{ij}) = ln(\bar{x}_i) + \epsilon_{ij} \ \ | \ \ \epsilon \sim N(0, a) \qquad (\textbf{Equation 1})$$

The sGOF graphics and numerical analyses supported that a log-constant error model best fit the data. The log-constant error model was not rejected for both the Kolmogorov-Smirnov test for normality (P = .22) nor the Pearson chi-square normality test (P = .0509). In contrast, a constant error model was rejected by these two tests (see **Figure S1** for further details).

<u>PK/PD Structural Model Building</u>

No outliers were identified during initial data exploration. Therefore, no collected data were excluded from model building.

The pharmacokinetics of bevacizumab, pemetrexed, and cisplatin were each modeled using one-compartment models with first order IP absorption and first order elimination based on literature descriptions and PK parameter estimates(23–25). Random effects (i.e. η_{pk}) were set to 0 as individual PK was not reported in these experiments.

A Gompertz function (**Equation 2**) was found to best describe the unperturbed tumor growth $V(t)$, based on its fit performance over competing models, low RSE on parameter estimates, and literature-established descriptive quality.

$$\left(\alpha - \beta \cdot \ln(V/V_c)\right) \cdot V \qquad (\textbf{Equation 2})$$

Due to sparseness in sampling, more complex semi-mechanistic models of growth were not supported by the data. Parameters α and β represent the proliferation rate of the tumor cells and rate of exponential decrease of the tumor relative growth rate, respectively. V_C is the unit value of relative fluorescence units (RFU) corresponding to one cell, i.e. the proportionality constant between RFU and the number of cancer cells in the fluorescent volume.

V_C was estimated externally from Monolix by conducting a naive-pooled, linear-regression on the natural-log of the full dataset. The regression gave a rough estimate of V_0 which was then scaled by the approximate number of cells injected at time 0 (ca. 120,000 cells) to derive $V_C = 5.064 \times 10^{-4}$ RFU.

After selecting an appropriate growth model, the log-kill effects of pemetrexed, cisplatin, and bevacizumab were each considered in parallel. The log-kill effect of bevacizumab was estimated as insignificant and removed from the model. The estimation of the log-kill effect of pemetrexed and cisplatin were found to be highly correlated. To reduce model complexity, only their combined concentration, $C(t)$, and a corresponding log-kill parameter, γ, were considered in the final model (**Equation 3**).

$$
\begin{bmatrix} \tau \\ Q(t) \\ \dot{V} \\ \dot{Z}_1 \\ \dot{Z}_2 \\ \dot{Z}_3 \\ N \end{bmatrix} = \begin{bmatrix} \tau_{bound} \cdot 10 \\ 1 + \delta \cdot A(t - \tau) \\ (\alpha - \beta \cdot \ln(V/V_c)) \cdot V - \gamma QCV \\ \gamma QCV - k \cdot Z_1 \\ k \cdot (Z_1 - Z_2) \\ k \cdot (Z_2 - Z_3) \\ V + Z_1 + Z_2 + Z_3 \end{bmatrix}, \begin{bmatrix} - \\ - \\ V(0) = V_0 \\ Z_1(0) = 0 \\ Z_2(0) = 0 \\ Z_3(0) = 0 \\ - \end{bmatrix}
$$

(Equation 3)

$A(t)$ represents the plasma concentration of bevacizumab. $Q(t)$ represents the synergistic effect of improved vascular quality. In brief, the increase in neoplasm vascular quality due to bevacizumab typically occurs within a period of a few days after administration. To represent this delay in effect, time (t) was delayed by τ. Parameter δ represents the proportional increase in PEM/CIS efficacy due to vascular quality improvement under bevacizumab therapy.

The estimation of τ was bounded between 0 and 10 using the link function $\tau = \tau_{bound} \cdot 10$, where $logit(\tau_{bound}) \sim N(0,1)$. All other parameters were best estimated as log-normally distributed. The full statistical representation of individual parameters, ϕ_i, estimated via SAEM is shown in **Equation 4**, where the full structural model is denoted by F.

(Equation 4)

$$
y_{ij} = F(\Phi_i, t_{ij}) \cdot e^{a\, \varepsilon_{ij}}, \qquad j \in \{1, \dots, n_i\}
$$

$$
\phi_i = \begin{bmatrix} \alpha_i = \alpha_{pop} \cdot e^{\eta_{\alpha,i}} \\ \beta_i = \beta_{pop} \cdot e^{\eta_{\beta,i}} \\ \gamma_i = \gamma_{pop} \cdot e^{\eta_{\gamma,i}} \\ \delta_i = \delta_{pop} \cdot e^{\eta_{\delta,i}} \\ logit(\tau_{bound_i}) = logit(\tau_{bound_{pop}}) + \eta_{\tau_{bound},i} \\ V_{0_i} = V_{0_{pop}} \cdot e^{\eta_{V0,i}} \\ k_i = k_{pop} \end{bmatrix}, \qquad i \in \{1, \dots, N\}
$$

Cellular death due to chemotherapeutic treatment was modeled as a three-compartment transition from the growth compartment to death(27). The compartments are labeled Z_1, Z_2, and Z_3 (numbering respective to their order) and transition between compartments is governed by intercompartmental clearance parameter k.

k was not identifiable using the SAEM algorithm. Thus, after a period of manual exploration, k was set to the value of 0.3. This choice is consistent with the parameterization made in Imbs et al(17). This choice also limits the total transition time from the tumor mass compartment to cellular death to the order of a day which is consistent with upper limits of cellular death clearance(31).

The full tumor size, N, was the sum of the size of unperturbed cells, V, as well as the size of damaged cells undergoing cellular death i.e. $Z_1 + Z_2 + Z_3$.

No correlations between random effects were statistically significant enough to be included in the final model (**Figure S2**). Full parameter estimates and model diagram are provided in **Table 1** and **Figure 1** respectively. Model diagnostics are collected in **Figure 2** through **Figure 4**.

<u>Simulations</u>

Simulating the experimental treatments with a range of administration gaps from 0 to 10 days (step-size = 0.1 day) suggested that the optimal time delay between scheduling bevacizumab and PEM/CIS in mice is 2.0 days (**Simulation set 1**).

The simulated IIV of the optimal gap was relatively small. Only three values of *individual* optimal gap were produced. 96.5% of the virtual animals had an *individual* optimal gap of 2.0 days, 1.0% of the virtual animals had an *individual* optimal gap of 2.1 days, and 2.5% of virtual animals had an *individual* gap of 1.9 days (**Simulation set 2**).

Scaling the dosage of bevacizumab to either 30 mg/kg or 10 mg/kg produced no effect in the estimated optimal gap and produced no effect in the IIV of the optimal gap (**Simulation set 3**).

Simulations of the typical human response to chemotherapy and bevacizumab were performed using IV administration, two-compartment absorption, and first order elimination models and parameters(32–34). Dosage and frequency of administration recommendations for BEV-PEM/CIS were adapted from DailyMed, a product label database maintained by the U.S. National Library of Medicine(35). Average adult weight and BSA were obtained from Center for Disease Control and literature estimates respectively(36,37).

Except for the proliferation rate of the tumor cells and rate of exponential decrease of the tumor relative growth rate (i.e. α and β), the PD model and parameterization were reused exactly as they were determined in the mouse portion of the model. α and β estimates were obtained from Bilous et al. 2018(38), where clinical NSCLC doubling times reported in Friberg and Mattson, 1998(39) were used to estimate population α and β for NSCLC in humans. The value of V_C came from the classical assumption that a 1 mm^3 volume of tumor cells is approximately 10^6 cells(40). V_0 was arbitrarily set to 3 cm^3.

The full PK/PD model was then used to simulate the typical cancer growth under various administration schedules with a starting tumor volume of 3 cm^3. Parameter estimates are reported in **Table 2** and simulation summaries are depicted in **Figure 5**. The estimated optimal gap between bevacizumab and PEM/CIS administration in humans was 1.2 days.

Discussion

By normalizing tumor vasculature, bevacizumab improves delivery of PEM/CIS to tumors which increases PEM/CIS anti-tumor efficacy. Pemetrexed and cisplatin each have a narrow therapeutic window, low clearance, and high toxicity. It is therefore critical that BEV-PEM/CIS doses are administered as efficiently as possible. This makes BEV-PEM/CIS a natural fit for modeling and simulation studies, as the drug scheduling can be optimized without the need for multiple time and resource intensive *in vivo* studies. In this analysis we conducted an *in silico* study of the optimal administration of BEV-PEM/CIS in a xenograft, and human, model of NSCLC by constructing a mathematical model of tumor dynamics in response to BEV-PEM/CIS. In constructing that model, we were able to validate and refine previous modeling in BEV-PEM/CIS. Greater precision in parameter estimates was achieved through external estimation of V_c, external validation of the residual error model, as well as using the larger fluorescence dataset to obtain final parameter estimates. Then, after exploring a range of predictions in mice, we scaled our model to predict optimal scheduling in humans.

The molecular profile of xenografts has a high degree of similarity with the molecular profile of the primary tumors from which the xenograft was derived(41) This indicates that there is compositional heterogeneity between xenografts and primary tumors. In addition, human NSCLC H460 cells are an experimentally established paradigm for modeling NSCLC tumors(42–44). Xenografts were grown after subcutaneous implantation in the mice flank, and not directly in the lungs. This is because monitoring tumor growth of lung orthotopic xenografts

with non-invasive techniques is limitingly difficult due to both the rapid movements of the chest in mice during imaging, and photon emission attenuation by the high amount of water in lung tissues. Consequently, ectopic xenografts were considered as the more robust experimental model for data collection. Taken together, these considerations motivated our choice of experimental model and are the basis for which we scaled our mathematical model for making predictions in humans.

In the error modeling portion of the experiment, we demonstrated a strategy through which the choice of the error model can be validated externally to the primary dataset by including supplementary data collection in the experimental design. This simplified the error modeling step in the model building process.

The next stage of this study consisted of determining whether the semi-mechanistic model of tumor dynamics in response to BEV-PEM/CIS developed in Imbs et al. 2017(17) best fit the unfit fluorescence data from the same study. During model building, we attempted to balance our model building procedure between model performance (empirical fit) and the underlying biology, an approach often referred to as the *middle-out* approach(45,46).

In selecting potential PD models of tumor growth, several semi-mechanistic models were fit to the experimental data. The Gompertz model and linear-exponential model performed comparably. The parameters of the Gompertz model were estimated with greater precision than the parameters of the linear-exponential model (RSE) where the linear-exponential model was fit with a lower BIC than the Gompertz model. Ultimately, the Gompertz model was chosen over the linear exponential model due to the physiological relevance of its construction.

The parameterization of the final model was slightly unstable due to modest overparameterization. To compensate for this, k was fixed to a reasonable physiological estimate to improve precision of parameter estimates, and the search for τ was upper bounded to reduce spurious individual parameter estimates. In addition, the direct anti-proliferative effect of bevacizumab, and individual effects of pemetrexed and cisplatin, respectively, were removed from the model.

The modeling phase of the study resulted in several validations of previous findings. First, we confirmed the validity of the mathematical model previously published in Imbs et al. 2017(17),

which we fit to our dataset. In doing so, we reconfirmed the ability of the model to describe BEV-PEM/CIS scheduling. We also reconfirmed the efficacy improvement of BEV-PEM/CIS dosing over PEM/CIS or control. We observed that a 3 day gap in scheduling is superior to both concomitant scheduling and an 8 day gap in scheduling. We were also able to build on previous work by identifying with greater precision the parameters underlying the mathematical model of BEV-PEM/CIS in NSCLC-tumor bearing mice.

In our mouse simulations, the final tumor volume (after 67 days) in the optimal scheduling group with BEV-PEM/CIS (gap = 2.0 days) was 88.5% of the size of final tumor volume in the concomitant scheduling group. This is consistent with our experimental results i.e. that mice administered bevacizumab approximately 2 days before PEM/CIS have a moderately better response (i.e. greater tumor size reduction) to BEV-PEM/CIS than mice who are administered BEV-PEM/CIS concomitantly.

The small magnitude of improvement in 2.0 day gap over concomitant scheduling is likely due to sub-optimal dosage and frequency of administration of BEV-PEM/CIS in the mice. We observed, by exploration, that a more robust preclinical response might be achieved by doubling the frequency of doses in mice and increasing the individual dosages by 50%.

We also found, through simulation, that scaling the dose of bevacizumab had no effect on the optimal gap and that IIV on gap is low.

Predictions made by our model agree with previous findings in BEV-PEM/CIS scheduling. The order of the optimal scheduling delay (2.0 days) is within the 1 to 5 day gap predictions of previous studies(12,18,19). Studies in tumor perfusion and bevacizumab showed Day 1 and Day 4 decrease in tumor perfusion which is consistent with the marginal predictions in our study i.e. optimal perfusion should be on the order of 2 days with comparable marginal losses on either side of that minimum(47).

After exploring various predictions in mice made by the model, the PK portion of the model was re-parameterized and the parameters of the PD portion of the model were scaled to simulate the relationship between varied administration schedules (i.e. gap) and efficacy in humans. Using this adapted parameterization, we estimated both optimal schedule of administration of BEV-PEM/CIS in humans and the marginal effects of a sub-optimal administration schedule of BEV-

PEM/CIS in humans (i.e. bevacizumab administered too many or too few days before PEM/CIS).

In our human simulations, we predicted a robust improvement in response to sequential BEV-PEM/CIS relative to concomitant scheduling. The final tumor volume (after 67 days) in the optimal scheduling group (gap = 1.2 days) was 30% of the size of the final tumor volume in the concomitant scheduling group. If these predictions are accurate, scheduling optimization could result in significant improvement in BEV-PEM/CIS CT efficacy with no increase in toxicity.

The predicted scale of the increase in efficacy after scheduling optimization was much greater in the human simulations than was either predicted by the mouse simulations, or was measured empirically in mice. This is at least partially due to the greater study that has been undertaken in optimizing dosages for human treatment of NSCLC. However, these promising estimates should not be substituted for clinical testing.

When exploring marginal efficacy loss in sub-optimal administration schedules, we consistently found that the marginal cost of scheduling bevacizumab and PEM/CIS too close together in time was greater than the marginal cost of scheduling bevacizumab and PEM/CIS with too great of a gap in administration - in both mice and humans. This indicates that any potential clinical studies in antiangiogenics and cytotoxics should weight scheduling recommendations toward scheduling at slightly too large of gap.

Finally, the tumor microenvironment is known to be complex and varied. Tumor tissues contain necrotic pockets, heterogenous and dynamic microvasculature, and various sub-mutations which result in differential local growth rate and drug sensitivity. Considering this biological heterogeneity would greatly improve future model predictions and scalability between species.

In summary, our analysis confirms previous findings in BEV-PEM/CIS scheduling while improving precision of parameter estimates, improving prediction quality and detail, and scaling the model to predict the optimal scheduling of BEV-PEM/CIS in humans.

Antiangiogenics will continue to be useful agents in oncology. There are currently several other antiangiogenics regularly used in combination with cytotoxics which could potentially benefit from sequential administration (i.e. antiangiogenic then cytotoxic)(48). Of note, bevacizumab is

currently only approved for concomitant administration with chemotherapy in all of its indications e.g. lung cancer, breast cancer, gastric cancer, etc. This contrasts with the optimized sequential scheduling that model simulations suggest.

There is a recent trend to develop model-informed drug development to optimize anticancer therapy. Our work highlights how mathematical modeling could help to refine clinical treatment modalities. The semi-mechanistic nature of this model allows it to be modularly reconfigured to extend predictions to other antiangiogenics as well as novel therapeutic paradigms such as the immune checkpoint inhibitor, monoclonal antibody pembrolizumab(49). This work continues to lay the foundation for building systems pharmacology models of the effect of antiangiogenic and antiproliferative combination therapy in advanced NSCLC. Tortuous vasculature is a phenotype exhibited by many solid tumors, and predicting optimal antiangiogenic scheduling could greatly increase the efficacy of future oncology therapeutics and combination therapies(50).

Acknowledgements

References

1. Barlesi F, Scherpereel A, Gorbunova V, Gervais R, Vikström A, Chouaid C, et al. Maintenance bevacizumab–pemetrexed after first-line cisplatin–pemetrexed–bevacizumab for advanced nonsquamous nonsmall-cell lung cancer: updated survival analysis of the AVAPERL (MO22089) randomized phase III trial. Ann Oncol. 2014 May 1;25(5):1044–52.

2. Barlesi F, Scherpereel A, Rittmeyer A, Pazzola A, Ferrer Tur N, Kim J-H, et al. Randomized Phase III Trial of Maintenance Bevacizumab With or Without Pemetrexed After First-Line Induction With Bevacizumab, Cisplatin, and Pemetrexed in Advanced Nonsquamous Non–Small-Cell Lung Cancer: AVAPERL (MO22089). Journal of Clinical Oncology. 2013 Aug 20;31(24):3004–11.

3. Galetta D, Cinieri S, Pisconti S, Gebbia V, Morabito A, Borsellino N, et al. Cisplatin/Pemetrexed Followed by Maintenance Pemetrexed Versus Carboplatin/Paclitaxel/Bevacizumab Followed by Maintenance Bevacizumab in Advanced Nonsquamous Lung Cancer: The GOIM (Gruppo Oncologico Italia Meridionale) ERACLE Phase III Randomized Trial. Clinical Lung Cancer. 2015 Jul 1;16(4):262–73.

4. Adjei AA. Pharmacology and Mechanism of Action of Pemetrexed. Clinical Lung Cancer. 2004 Apr 1;5:S51–5.

5. Poklar N, Pilch DS, Lippard SJ, Redding EA, Dunham SU, Breslauer KJ. Influence of cisplatin intrastrand crosslinking on the conformation, thermal stability, and energetics of a 20-mer DNA duplex. PNAS. 1996 Jul 23;93(15):7606–11.

6. Rudd GN, Hartley JA, Souhami RL. Persistence of cisplatin-induced DNA interstrand crosslinking in peripheral blood mononuclear cells from elderly and young individuals. Cancer Chemother Pharmacol. 1995 Jul 1;35(4):323–6.

7. Dasari S, Tchounwou PB. Cisplatin in cancer therapy: molecular mechanisms of action. Eur J Pharmacol. 2014 Oct 5;0:364–78.

8. Chen K-C, Yang T-Y, Wu C-C, Cheng C-C, Hsu S-L, Hung H-W, et al. Pemetrexed Induces S-Phase Arrest and Apoptosis via a Deregulated Activation of Akt Signaling Pathway. PLoS One [Internet]. 2014 May 21 [cited 2019 Jan 14];9(5). Available from: https://www.ncbi.nlm.nih.gov/pmc/articles/PMC4029963/

9. Wagner JM, Karnitz LM. Cisplatin-Induced DNA Damage Activates Replication Checkpoint Signaling Components that Differentially Affect Tumor Cell Survival. Mol Pharmacol. 2009 Jul;76(1):208–14.

10. Ferrara N, Hillan KJ, Gerber H-P, Novotny W. Discovery and development of bevacizumab, an anti-VEGF antibody for treating cancer. Nature Reviews Drug Discovery. 2004 May;3(5):391–400.

11. Jain RK. Normalizing tumor vasculature with anti-angiogenic therapy: A new paradigm for combination therapy. Nature Medicine. 2001 Sep;7(9):987–9.

12. Tong RT, Boucher Y, Kozin SV, Winkler F, Hicklin DJ, Jain RK. Vascular Normalization by Vascular Endothelial Growth Factor Receptor 2 Blockade Induces a Pressure Gradient

Across the Vasculature and Improves Drug Penetration in Tumors. Cancer Research. 2004 Jun 1;64(11):3731–6.

13. Jain RK. Antiangiogenesis Strategies Revisited: From Starving Tumors to Alleviating Hypoxia. Cancer Cell. 2014 Nov;26(5):605–22.

14. Kerbel RS. Antiangiogenic Therapy: A Universal Chemosensitization Strategy for Cancer? Science. 2006 May 26;312(5777):1171–5.

15. Tolaney SM, Boucher Y, Duda DG, Martin JD, Seano G, Ancukiewicz M, et al. Role of vascular density and normalization in response to neoadjuvant bevacizumab and chemotherapy in breast cancer patients. PNAS. 2015 Nov 17;112(46):14325–30.

16. Crawford J, Becker PS, Armitage JO, Blayney DW, Chavez J, Curtin P, et al. Myeloid Growth Factors, Version 2.2017, NCCN Clinical Practice Guidelines in Oncology. J Natl Compr Canc Netw. 2017 Dec 1;15(12):1520–41.

17. Imbs D-C, Cheikh RE, Boyer A, Ciccolini J, Mascaux C, Lacarelle B, et al. Revisiting Bevacizumab + Cytotoxics Scheduling Using Mathematical Modeling: Proof of Concept Study in Experimental Non-Small Cell Lung Carcinoma. CPT: Pharmacometrics & Systems Pharmacology. 2018;7(1):42–50.

18. Dickson PV, Hamner JB, Sims TL, Fraga CH, Ng CYC, Rajasekeran S, et al. Bevacizumab-Induced Transient Remodeling of the Vasculature in Neuroblastoma Xenografts Results in Improved Delivery and Efficacy of Systemically Administered Chemotherapy. Clin Cancer Res. 2007 Jul 1;13(13):3942–50.

19. Winkler F, Kozin SV, Tong RT, Chae S-S, Booth MF, Garkavtsev I, et al. Kinetics of vascular normalization by VEGFR2 blockade governs brain tumor response to radiation: Role of oxygenation, angiopoietin-1, and matrix metalloproteinases. Cancer Cell. 2004 Dec 1;6(6):553–63.

20. Ciccolini J, Benzekry S, Lacarelle B, Barbolosi D, Barlési F. Improving efficacy of the combination between antiangiogenic and chemotherapy: Time for mathematical modeling support. PNAS. 2015 Jul 7;112(27):E3453–E3453.

21. Benzekry S, Chapuisat G, Ciccolini J, Erlinger A, Hubert F. A new mathematical model for optimizing the combination between antiangiogenic and cytotoxic drugs in oncology. Comptes Rendus Mathematique. 2012 Jan;350(1–2):23–8.

22. Lignet F, Benzekry S, Wilson S, Billy F, Saut O, Tod M, et al. Theoretical investigation of the efficacy of antiangiogenic drugs combined to chemotherapy in xenografted mice. Journal of Theoretical Biology. 2013 Mar;320:86–99.

23. Johnsson A, Olsson C, Nygren O, Nilsson M, Seiving B, Cavallin-Stahl E. Pharmacokinetics and tissue distribution of cisplatin in nude mice: platinum levels and cisplatin-DNA adducts. Cancer Chemotherapy and Pharmacology. 1995;37(1–2):23–31.

24. Lin YS, Nguyen C, Mendoza J-L, Escandon E, Fei D, Meng YG, et al. Preclinical Pharmacokinetics, Interspecies Scaling, and Tissue Distribution of a Humanized Monoclonal Antibody against Vascular Endothelial Growth Factor. 1999;288:8.

25. Woodland JM, Barnett CJ, Dorman DE, Gruber JM, Shih C, Spangle LA, et al. Metabolism and Disposition of the Antifolate LY231514 in Mice and Dogs. Drug Metab Dispos. 1997 Jun 1;25(6):693–700.

26. Benzekry S, Lamont C, Beheshti A, Tracz A, Ebos JML, Hlatky L, et al. Classical Mathematical Models for Description and Prediction of Experimental Tumor Growth. PLOS Computational Biology. 2014 Aug 28;10(8):e1003800.

27. Simeoni M, Magni P, Cammia C, Nicolao GD, Croci V, Pesenti E, et al. Predictive Pharmacokinetic-Pharmacodynamic Modeling of Tumor Growth Kinetics in Xenograft Models after Administration of Anticancer Agents. Cancer Res. 2004 Feb 1;64(3):1094–101.

28. Lavielle M, Ribba B. Enhanced Method for Diagnosing Pharmacometric Models: Random Sampling from Conditional Distributions. Pharmaceutical Research. 2016 Dec;33(12):2979–88.

29. Pelligand L, Soubret A, King JN, Elliott J, Mochel JP. Modeling of Large Pharmacokinetic Data Using Nonlinear Mixed-Effects: A Paradigm Shift in Veterinary Pharmacology. A Case Study With Robenacoxib in Cats. CPT: Pharmacometrics & Systems Pharmacology. 2016;5(11):625–35.

30. Lavielle M. mlxR: Simulation of Longitudinal Data [Internet]. 2018 [cited 2019 Jan 22]. Available from: https://CRAN.R-project.org/package=mlxR

31. Spencer SL, Sorger PK. Measuring and Modeling Apoptosis in Single Cells. Cell. 2011 Mar 18;144(6):926–39.

32. Latz JE, Chaudhary A, Ghosh A, Johnson RD. Population pharmacokinetic analysis of ten phase II clinical trials of pemetrexed in cancer patients. Cancer Chemother Pharmacol. 2006 Apr 1;57(4):401–11.

33. Lu J-F, Bruno R, Eppler S, Novotny W, Lum B, Gaudreault J. Clinical pharmacokinetics of bevacizumab in patients with solid tumors. Cancer Chemother Pharmacol. 2008 Oct 1;62(5):779–86.

34. Urien S, Brain E, Bugat R, Pivot X, Lochon I, Van M-LV, et al. Pharmacokinetics of platinum after oral or intravenous cisplatin: a phase 1 study in 32 adult patients. Cancer Chemother Pharmacol. 2005 Jan 1;55(1):55–60.

35. U.S. National Library of Medicine. DailyMed [Internet]. DailyMed. [cited 2019 Jan 14]. Available from: https://dailymed.nlm.nih.gov/dailymed/index.cfm

36. McDowell MA, Fryar CD, Ogden CL, Flegal KM. Anthropometric Reference Data for Children and Adults: United States, 2003-2006: (623932009-001) [Internet]. American Psychological Association; 2008 [cited 2019 Jan 14]. Available from: http://doi.apa.org/get-pe-doi.cfm?doi=10.1037/e623932009-001

37. Sacco JJ, Botten J, Macbeth F, Bagust A, Clark P. The Average Body Surface Area of Adult Cancer Patients in the UK: A Multicentre Retrospective Study. Shea BJ, editor. PLoS ONE. 2010 Jan 28;5(1):e8933.

38. Bilous M, Serdjebi C, Boyer A, Tomasini P, Pouypoudat C, Barbolosi D, et al. Computational modeling reveals dynamics of brain metastasis in non-small cell lung cancer and provides a tool for personalized therapy. bioRxiv [Internet]. 2018 Oct 19 [cited 2019 Jan 14]; Available from: http://biorxiv.org/lookup/doi/10.1101/448282

39. Friberg S, Mattson S. On the growth rates of human malignant tumors: Implications for medical decision making. Journal of Surgical Oncology. 1997;65(4):284–97.

40. Spratt JS, Meyer JS, Spratt JA. Rates of growth of human solid neoplasms: Part I. Journal of Surgical Oncology. 1995 Oct;60(2):137–46.

41. Wang D, Pham N-A, Tong J, Sakashita S, Allo G, Kim L, et al. Molecular heterogeneity of non-small cell lung carcinoma patient-derived xenografts closely reflect their primary tumors. International Journal of Cancer. 2017;140(3):662–73.

42. Li H, Takayama K, Wang S, Shiraishi Y, Gotanda K, Harada T, et al. Addition of bevacizumab enhances antitumor activity of erlotinib against non-small cell lung cancer xenografts depending on VEGF expression. Cancer Chemother Pharmacol. 2014;74(6):1297–305.

43. NUKATSUKA M, SAITO H, NAKAGAWA F, TSUJIMOTO H, SAKAMOTO K, TSUKIOKA S, et al. Combination therapy using oral S-1 and targeted agents against human tumor xenografts in nude mice. Exp Ther Med. 2012 May;3(5):755–62.

44. Xu Y, Chang E, Liu H, Jiang H, Gambhir SS, Cheng Z. Proof-of-Concept Study of Monitoring Cancer Drug Therapy with Cerenkov Luminescence Imaging. J Nucl Med. 2012 Feb;53(2):312–7.

45. Li R, Barton HA, Yates PD, Ghosh A, Wolford AC, Riccardi KA, et al. A "middle-out" approach to human pharmacokinetic predictions for OATP substrates using physiologically-based pharmacokinetic modeling. Journal of Pharmacokinetics and Pharmacodynamics. 2014 Jun;41(3):197–209.

46. Bon C, Toutain PL, Concordet D, Gehring R, Martin-Jimenez T, Smith J, et al. Mathematical modeling and simulation in animal health. Part III: Using nonlinear mixed-effects to characterize and quantify variability in drug pharmacokinetics. Journal of Veterinary Pharmacology and Therapeutics. 2018 Apr;41(2):171–83.

47. Van der Veldt AAM, Lubberink M, Bahce I, Walraven M, de Boer MP, Greuter HNJM, et al. Rapid Decrease in Delivery of Chemotherapy to Tumors after Anti-VEGF Therapy: Implications for Scheduling of Anti-Angiogenic Drugs. Cancer Cell. 2012 Jan 17;21(1):82–91.

48. Gougis P, Wassermann J, Spano JP, Keynan N, Funck-Brentano C, Salem JE. Clinical pharmacology of anti-angiogenic drugs in oncology. Critical Reviews in Oncology/Hematology. 2017 Nov 1;119:75–93.

49. Pai-Scherf L, Blumenthal GM, Li H, Subramaniam S, Mishra-Kalyani PS, He K, et al. FDA Approval Summary: Pembrolizumab for Treatment of Metastatic Non-Small Cell Lung Cancer: First-Line Therapy and Beyond. Oncologist. 2017 Nov;22(11):1392–9.

50. Reck M, Rodríguez-Abreu D, Robinson AG, Hui R, Csőszi T, Fülöp A, et al. Pembrolizumab versus Chemotherapy for PD-L1–Positive Non–Small-Cell Lung Cancer. New England Journal of Medicine. 2016 Nov 10;375(19):1823–33.

Table 1 Pharmacodynamic Model Parameters for Tumor Proliferation in NSCLC-Xenografted Mice
Model parameter estimates (fixed and random-effects) as well as standard errors as determined by the
Stochastic Approximation Expectation-Maximization algorithm as implemented in Monolix 2018R2.

Model Parameter	Estimate	SE	RSE (%)	IIV	IIV (CV%)
α	0.77 day^{-1}	0.0081	1.06	0.037	4.76
β	0.04 day^{-1}	0.0005	1.16	0.015	33.55
γ	35.74 (mg·day)$^{-1}$	6.36	17.79	0.46	1.28
δ	3.73 (mg·day)$^{-1}$	0.92	24.70	0.35	9.51
τ_{bound}	.119 days	0.0017	1.50	0.017	14.50
V_0	3.4 RFU*	0.27	22.55	1.73	143.03
k	0.30 days	-	-	-	-
Residual Error Variance	0.43	0.01	2.55	-	-

*RFU: Relative Fluorescence Unit

Table 2 <u>Model Parameterization for Simulations of NSCLC treated with BEV-PEM/CIS in Humans</u>
Except for the proliferation rate of the tumor cells and rate of exponential decrease of the tumor relative growth rate (i.e. α, β), the PD model and parameterization were reused exactly as they were determined in the mouse portion of the model. α and β estimates were obtained from Bilous et al. 2018(38), where clinical NSCLC doubling times reported in Friberg and Mattson, 1998(39) were used to estimate population α and β for NSCLC in humans. The value of V_c came from the classical assumption that a 1 mm³ volume of tumor cells is approximately 106 cells(40). V_0 was arbitrarily set to 3 cm³. $V, k_{m,n}$, and Q represent volume, compartmental clearance from compartment m to compartment n, and intercompartmental clearance respectively.

Pemetrexed Pharmacokinetics		Bevacizumab Pharmacokinetics		Pharmacodynamics	
$Clearance$	91.6 mL/min	$Clearance$	0.22 L/day	α	0.0284 day^{-1}
V_1	12.9 L	V_1	2.8 L	β	1.03E-3 day^{-1}
Q	14.4 mL/min	k_{12}	0.22 day^{-1}	γ	35.7 (mg·day)$^{-1}$
V_2	3.38 L	k_{21}	0.22 day^{-1}	δ	3.73 (mg·day)$^{-1}$
Cisplatin Pharmacokinetics				τ	1.19 days
$Clearance$	37.0 L/h			V_0	3 cm³
V_1	22.7 L			k	0.3 days
Q	10.7 L/h			V_c	10E-3 mm³·cell^{-1}
V_2	19.5 L				

Figure 1 Structural Model Diagram

The scheme of the structural model is depicted to the right. Unperturbed cells grow at rate governed by α and β. When a cytotoxic is introduced into the system, the cytotoxic impairs the growth of the tumor by sending cells into a death succession. The parameter which determines the cytotoxic efficacy, γ, is scaled by both the concentration of cytotoxics, $C(t)$, and the volume of the tumor, $V(t)$. Bevacizumab improves vascular quality, $Q(t)$, after time delay, τ, which scales the cytotoxic effect by parameter δ. When a cell is damaged by cytotoxics it begins a progression from unperturbed growth – compartment $V(t)$ – to damage compartments Z_1 through Z_1. Eventually the cell exits the tumor volume as it dies. The rate of transfer between damage compartments is governed by intercompartmental clearance parameter k.
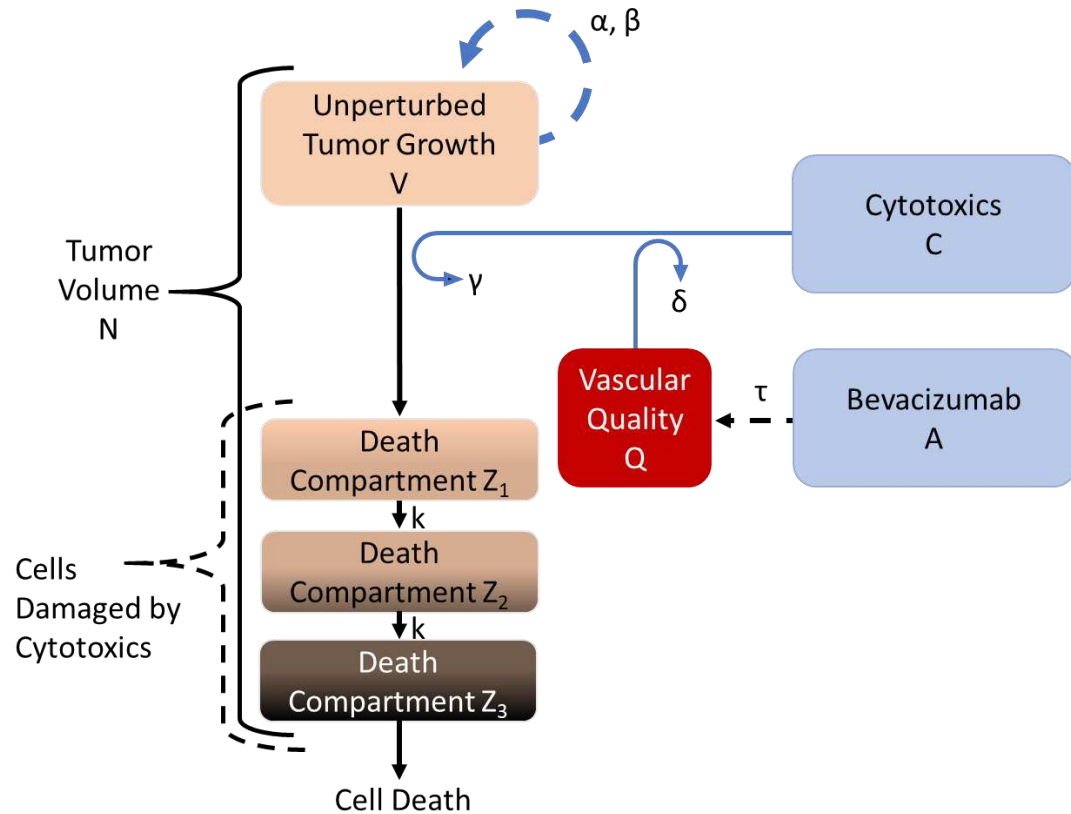
Figure 2 Standard Goodness-of-Fit Diagnostic Plots

On the left is individual predictions vs. observations and on the right are the individualized weighted residuals (IWRES) vs time. During model fitting, observations were natural-log-transformed to stabilize predictions. Therefore, residuals, predictions, and observations are natural-log-transformed in these figures. The predictions are approximately normally distributed. On the left, the one-to-one prediction line is the center solid black line, the spline (average agreement between individual prediction and observation) is solid orange, the dashed black lines are the borders of the 90% prediction interval. On the right, the zero residual error line is the center dashed black line, the spline is solid orange. The dashed black lines are the borders of the 90% prediction interval.
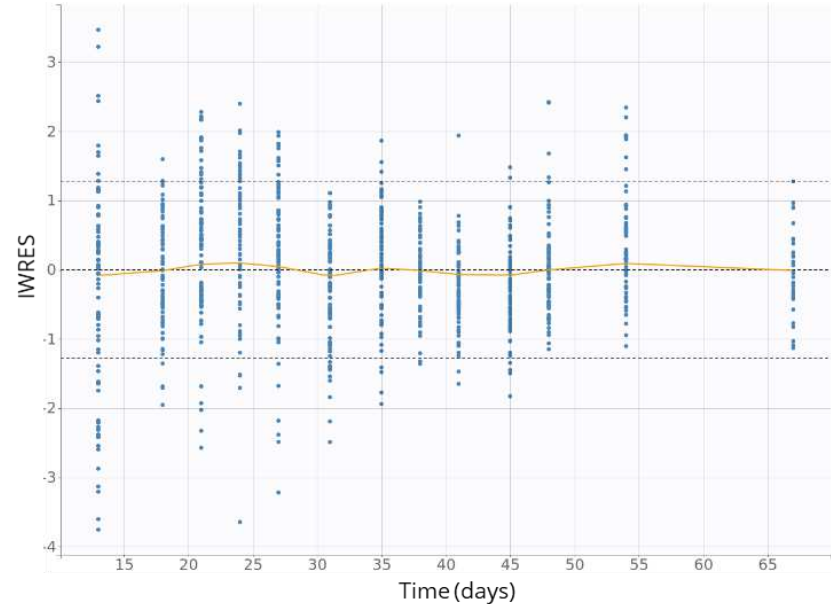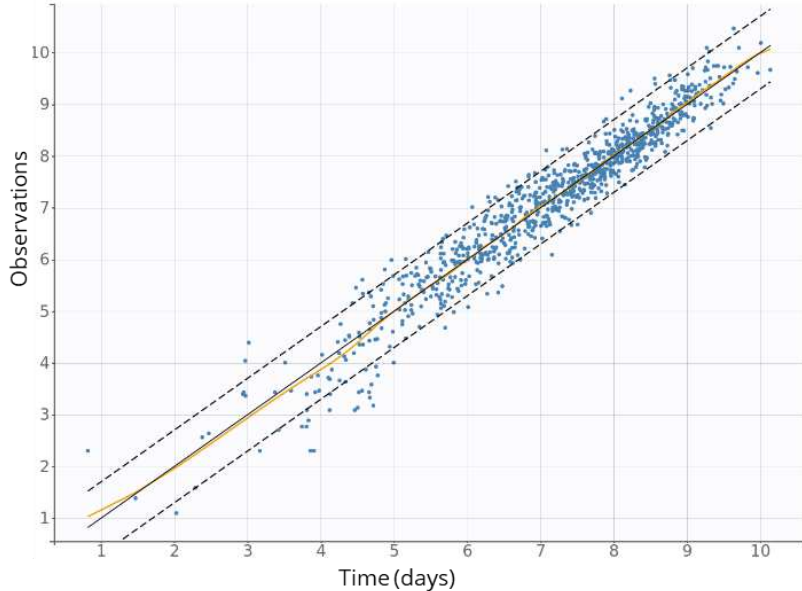
Figure 3 <u>Sample of Individual Fits</u>
The blue dots represent individual observations while the solid violet line represents individual fits.
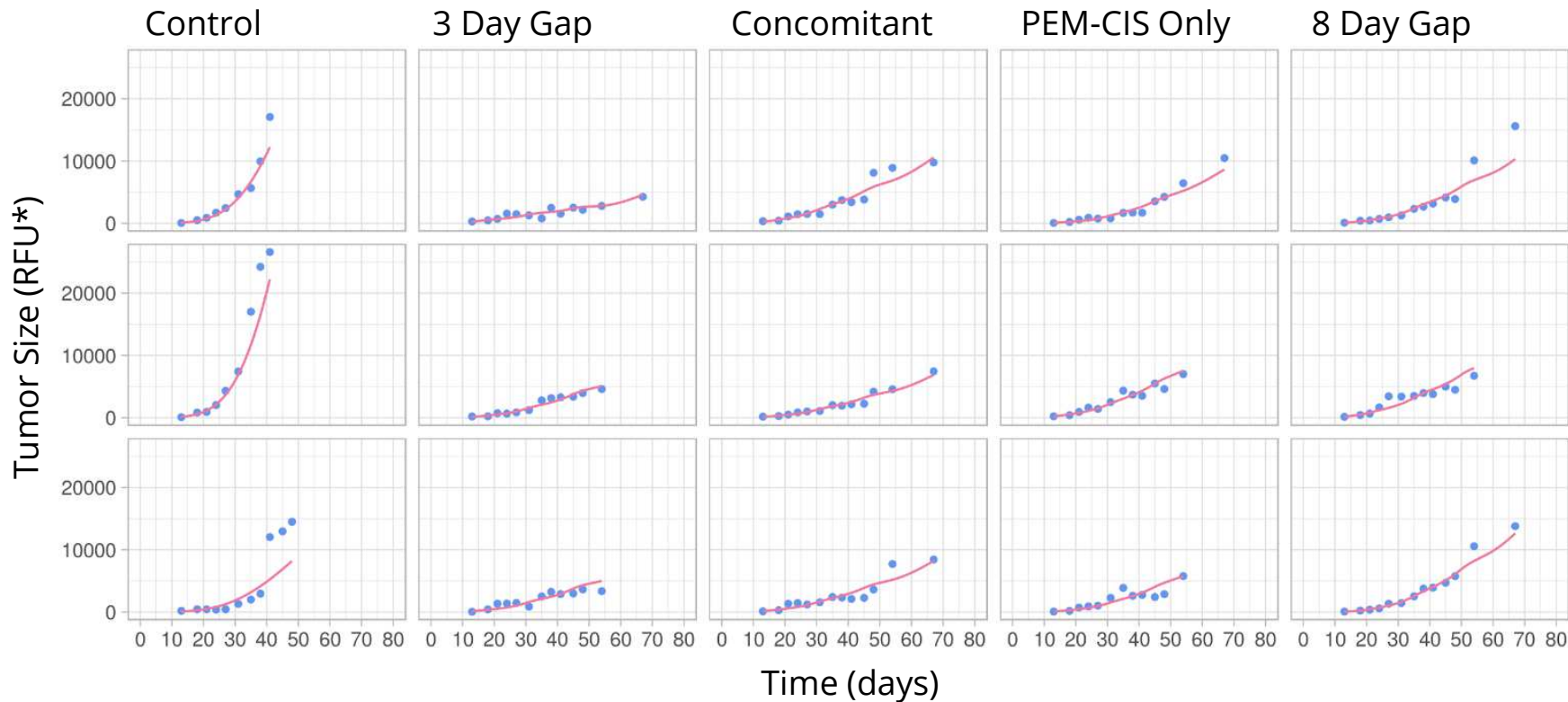
*RFU: Relative Fluorescence Unit

Figure 4 <u>Combined and Stratified Visual Predictive Checks</u>
The blue lines are the 10th, 50th, and 90th empirical percentiles calculated for each unique value of time.
Blue and pink areas represent 90% prediction intervals for the 10th (blue), 50th (pink), and 90th (blue)
percentiles. Prediction intervals are calculated by Monte Carlo simulation. To create prediction intervals for
each unique value of time, 500 simulations are performed using random individual parameters. The red
areas and red-circled points represent areas where empirical measurements fall outside of the bounds of
the 90% prediction intervals.

Figure 5 Human Pharmacodynamic and Pharmacodynamic Simulations Summary To produce these figures, bevacizumab (BEV) was administered anywhere from 0 to 10 days (in steps of 0.1) before pemetrexed/cisplatin (PEM/CIS) was administered. Tumor growth was simulated from 0 to 67 days with no IIV and no RSE. In the top figure, AUC of tumor growth vs gap (0 to 10 days) is depicted. In the middle figure, tumor dynamics over time, with gap indicated by color, are depicted. In the bottom panel, the PK of BEV-PEM/CIS is depicted with gap indicated by color. The top figure indicates that the optimal scheduling gap is 1.2 days and the middle figure depicts the difference in tumor volume between administration gaps. The patient with optimal scheduling had a final tumor volume approx. 30% the size of the concomitant scheduling.
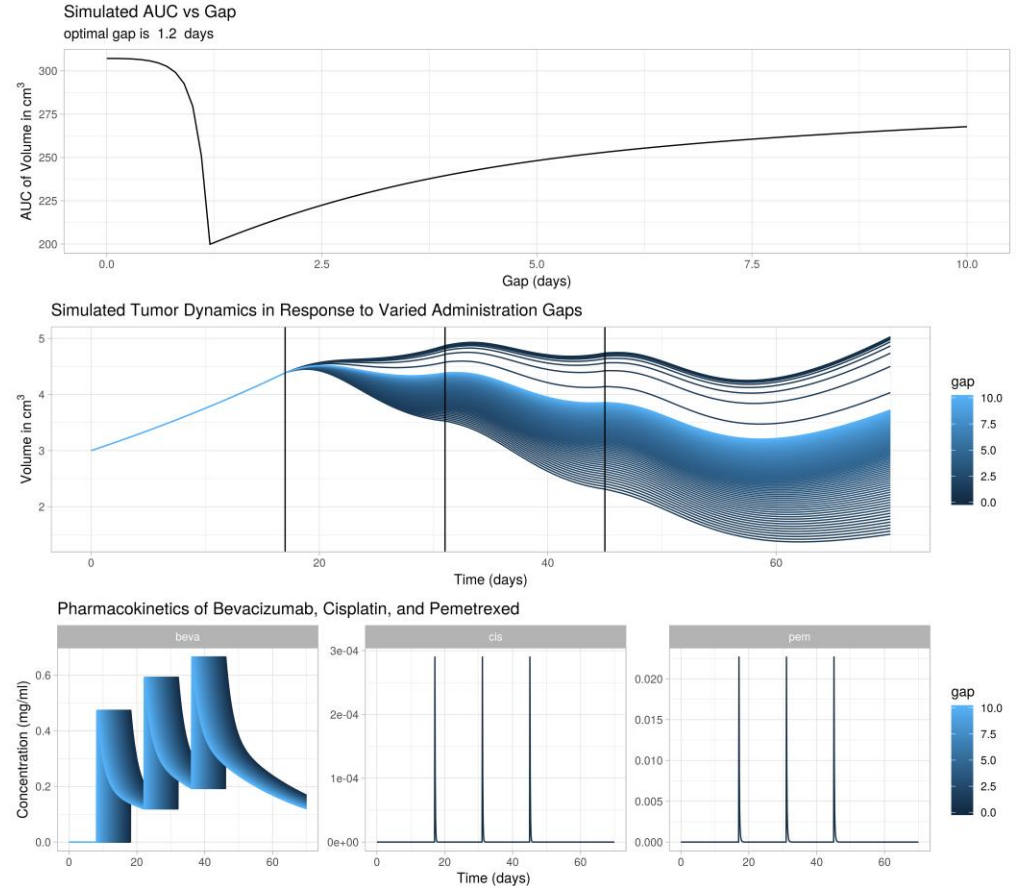
The patient with optimal scheduling had a final tumor volume 30.019 % the size of the concomitant scheduling.

Table S1 Administration (adm) schedule for the five experimental groups. The cytotoxics consisted of an administration of both 100 mg/kg of pemetrexed IP and 3 mg/kg of cisplatin IP. Bevacizumab was administered in doses of 20 mg/kg IP.

Group	Experimental Day of bevacizumab adm	Experimental Day of cytotoxics adm	Group Size
Control	-	-	15
Cytotoxic control	-	14, 28, 42	15
No gap in adm	14, 28, 42	14, 28, 42	16
Three day gap	11, 25, 39	14, 28, 42	15
Eight day gap	6, 20, 34	14, 28, 42	15

Table S2 Administration (adm) schedule for the simulated human individual. Drugs were administered on three separate occasions, the 17th, 31st, and 45th experimental day. Bevacizumab administration (adm) was varied between simulation run i.e. it was administered anywhere between 0 and 10 days before Pemetrexed-Cisplatin.

	Bevacizumab	Pemetrexed	Cisplatin
Adm Day 1 Experimental Day	17 - gap	17	17
Adm Day 2 Experimental Day	31 - gap	31	31
Adm Day 3 Experimental Day	45 - gap	45	45
Dose Given IV	15 mg/kg	100 mg/m^2 of BSA	500 mg/m^2 of BSA
Duration of Infusion	1 hours	7 hours	2 hours

Figure S1 In this figure the various error models are compared. In the left column are the probability density distributions (red) vs. theoretical normal distributions (blue) for each error group. On the right are the quantile-quantile plots which compare the quantiles between the theoretical and observed distributions of points. Below each set of sGOF graphics are the scores for the Kolomogorov-Smirnov normality test as well as the Pearson chi-square normality test. Graphically, the log-constant error model outperformed the constant error model. Numerically, the log-constant error model outperformed the constant error model in both the Kolmogorov-Smirnov normality test and the Pearson-Chi square test.
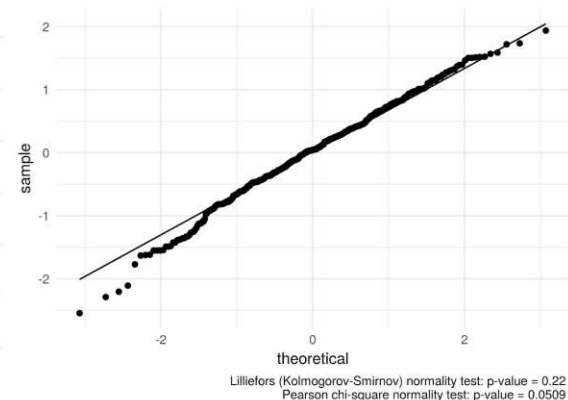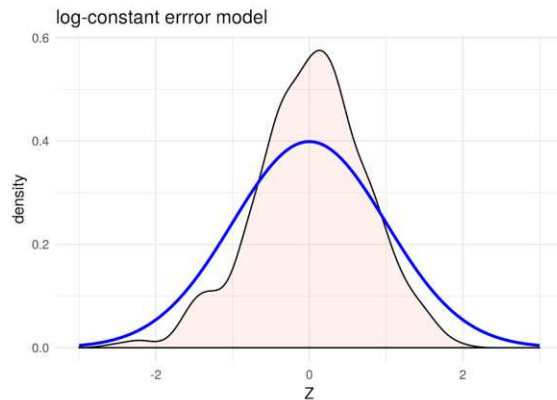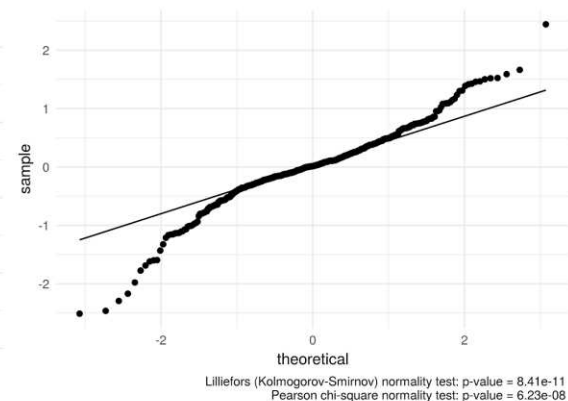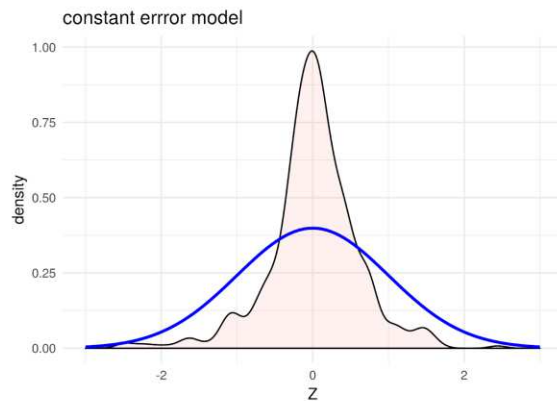
Figure S2 Correlation between parameter estimates. The Pearson's Correlation Coefficient is displayed in each correlation and the red line is the linear regression of the conditional distribution.
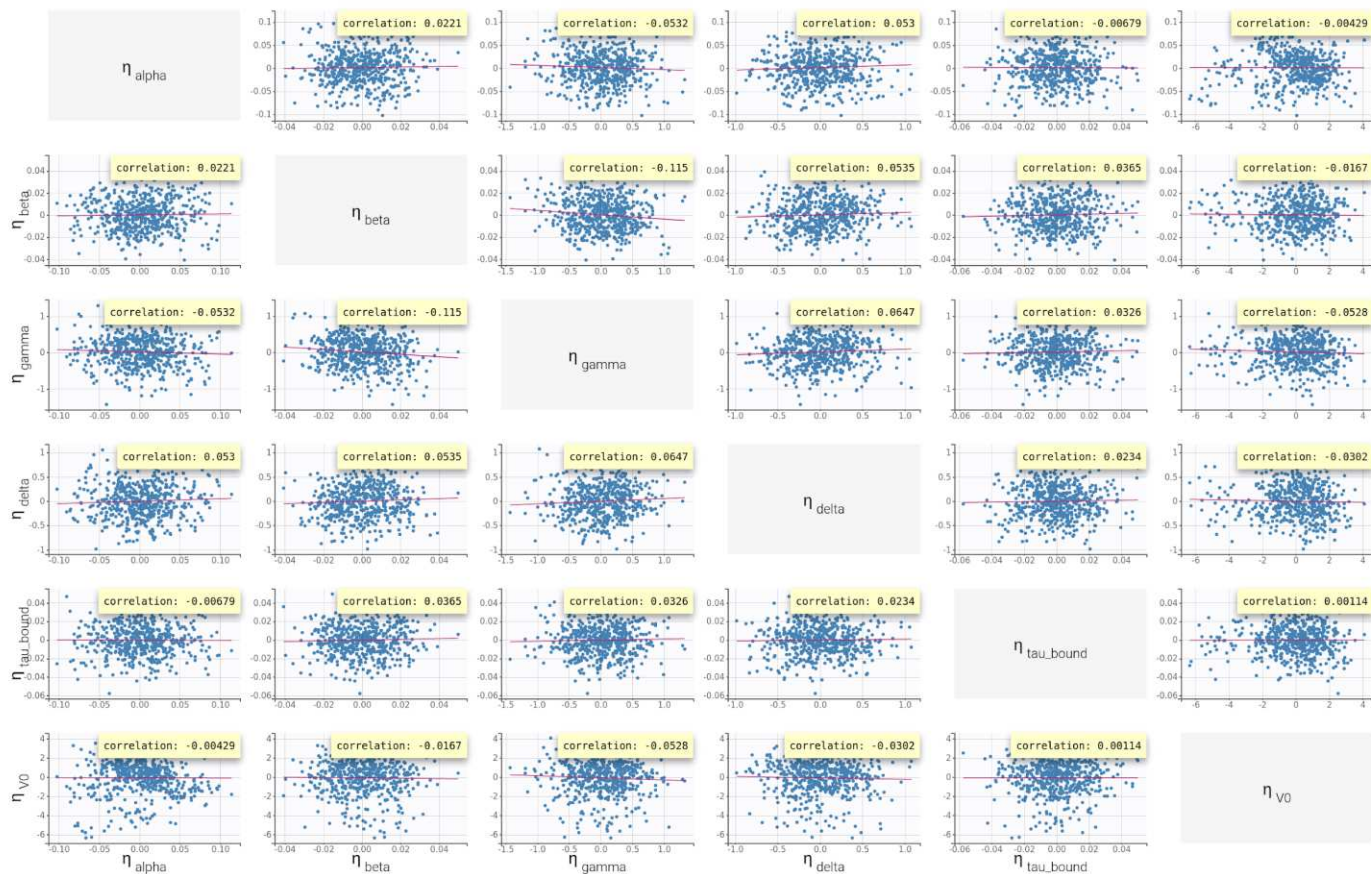
Figure S3 Below are various SAEM convergence results produced by Monolix's *assessment suite*. The best performing (defined as lowest *-2 loglikelihood*) parameterization (in yellow) closely matches our final parameter estimates. The assessment indicates that there is some degree of instability in parameter estimates. But, variance in parameter estimates is relatively low and RSE on final parameter estimates is low, indicating that we've achieved a reasonable balance between the empirical fit and underlying biology. Especially important to our analysis is the relatively low variability in Tau parameter estimates.
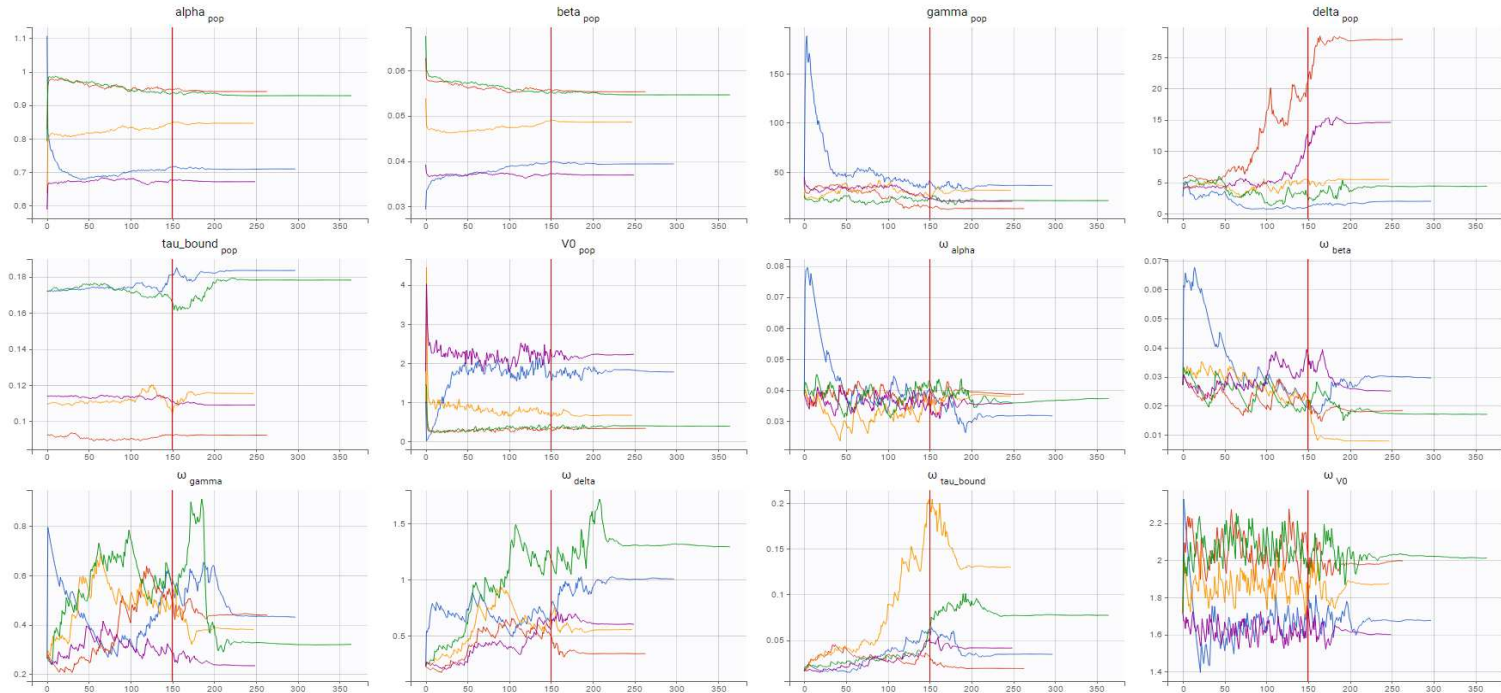
Figure S4 Below is the 3D surface of simulated tumor growth response (dimension 1) with respect to gap (dimension 2) and time (dimension 3) in mice. This 3D surface allowed us to more intuitively understand the effect of varied administration schedules. It is available for manipulation at https://plot.ly/~Benjamin-PKPD/15/#/.
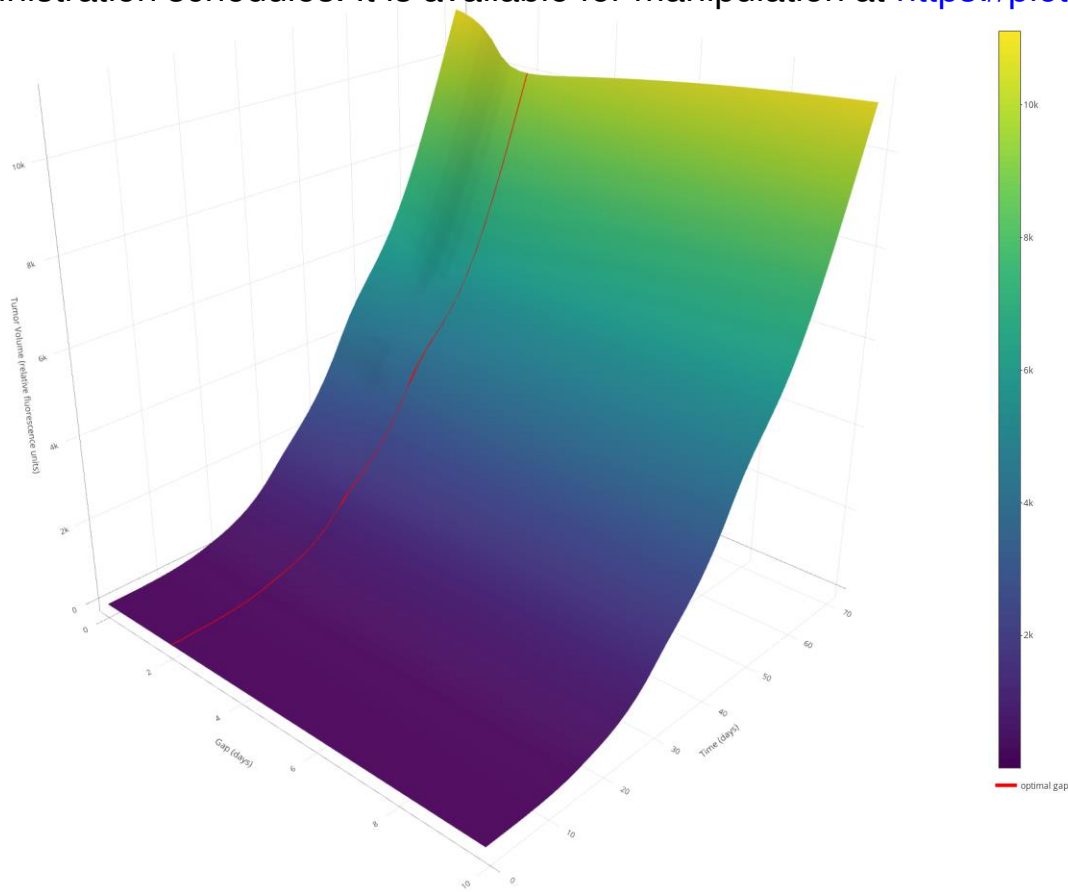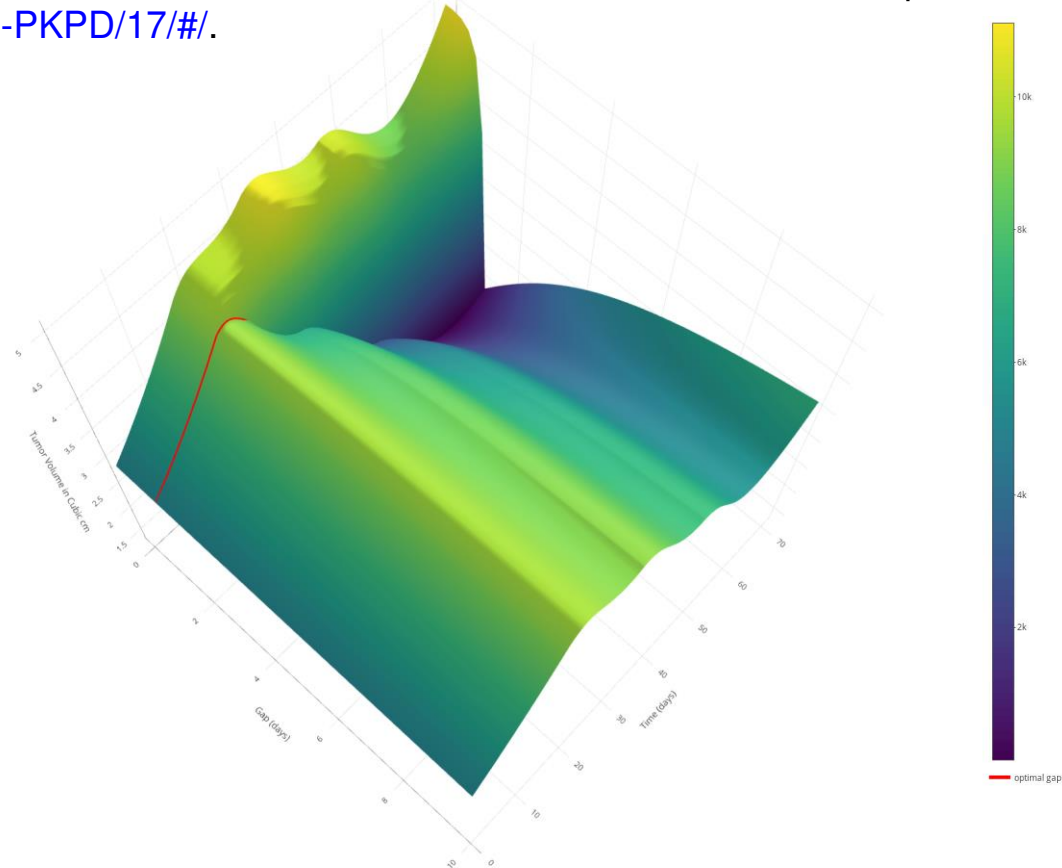
Figure S5 Below is the 3D surface of simulated tumor growth response (dimension 1) with respect to gap (dimension 2) and time (dimension 3) in humans. This 3D surface allowed us to more intuitively understand the effect of varied administration schedules. It is available for manipulation at https://plot.ly/~Benjamin-PKPD/17/#/.

Supplementary Methods: Simulation Details

In **simulation set 1**, population response was simulated with no IIV and without RSE. The simulated treatment schedule consisted of 100 mg/kg of pemetrexed IP and 3 mg/kg of cisplatin IP on Day 14, 28, and 42. 20 mg/kg IP of bevacizumab was virtually administered anywhere from 0 to 10 days (in steps of .1) before Day 14, 28, and 42. See **Table S2** for details.

The simulation was stopped after 67 virtual days. These simulations allowed the prediction of the optimal gap between administering bevacizumab and PEM-CIS. Efficacy of the drugs was assessed using AUC of the tumor growth over time as calculated by the spline method implemented in the R package DescTools 0.99.25[1]. The optimal gap was defined as the administration scheduling gap which resulted in the lowest AUC of tumor growth vs. time over the simulated time period ($t = 0$ to $t = 67$).

In **simulation set 2** the inter-individual variability of optimal gap was meticulously calculated using a virtual population of 1000 simulated mice. First, a set of parameters representing 1000 virtual mice was generated without RSE from the parameter distributions determined in the structural modeling phase. Then, the procedure from **simulation set 1** was replicated per individual to estimate each *individual* optimal gap. Finally, the distribution of *individual* optimal gaps was assessed using the mode, standard deviation, and range as well as graphical methods such as a violin plot of count density.

To produce **simulation set 3**, the procedure which generated **simulation set 1** was repeated with scaled doses of bevacizumab. First, 10 mg/kg IP of bevacizumab was substituted for 20 mg/kg IP of bevacizumab. Second, 30 mg/kg IP of bevacizumab substituted for 20 mg/kg IP of bevacizumab. This was done to assess the effect of bevacizumab dosage on the estimated optimal gap.

In **simulation set 4** an analogous treatment regimen to **simulation set 1** was simulated in a virtual NSCLC tumor-bearing human population using adapted human dosing recommendations. The random effects were set to zero and population response was simulated

---

[1]Aho ASIR source code and/or documentation previously published by (in alphabetical order): K, Alfons A, Anderegg N, et al. DescTools: Tools for Descriptive Statistics.; 2019. https://CRAN.R-project.org/package=DescTools. Accessed January 23, 2019.

without RSE. Therefore, our simulations represent the average effect of varied administration schedule.

The model used in **simulation set 4** was a scaling of the model fit obtained from the xenograft mouse model. The PK portion of the model was built and parameterized using previously published PK models and typical parameter values. The PD parameter estimates were obtained from both the xenograft mouse model and from literature values.

Tumor dynamics in response to PEM-CIS-BEV were simulated using a scheduling gap of 0 days to 10 days in steps of .1. A graphical representation of the AUC vs. administration gap was generated to determine the optimal gap between bevacizumab and PEM-CIS dosing.